ELSEVIER

Contents lists available at ScienceDirect

Materials Letters

journal homepage: www.elsevier.com/locate/matlet



Bi₂O₂S nanosheets for effective visible light photocatalysis of anionic dye degradation

Tank R. Seling ^a, Amit Kumar Shringi ^a, Ke Wang ^b, Ufana Riaz ^a, Fei Yan ^a

ARTICLE INFO

Keywords:
Bismuth oxysulfide
Photocatalysis
Dye degradation
Nanosheets

ABSTRACT

Herein, we introduce the first investigation into the photocatalytic properties of ultrathin Bi₂O₂S nanosheets prepared by a hydrothermal method. These nanosheets demonstrate exceptional efficiency in degrading congo red (CR) and rose bengal (RB) when exposed to visible light. The degradation rates reached approximately 82 % for CR and 80 % for RB, respectively. The rate constants for CR and RB degradation were found to be 1.8×10^{-2} min⁻¹ and 1.3×10^{-2} min⁻¹, respectively, during a 75 and 150-minute exposure to Bi₂O₂S nanosheets.

1. Introduction

The discharge of untreated wastewater from textile, pharmaceutical, dying and paper printing industries leads to an increased amount of dyes in the water sources, causing a severe threat to the environment [1,2]. To get rid of these dyes, various degradation approaches like membrane filtration, oxidation, adsorption and photocatalysis have been successfully developed and demonstrated [3,4]. Photocatalytic degradation is considered as the most preferred technique due to its degradation efficiency, free photon energy and simple process. A variety of nanomaterials including metal oxide, chalcogenides, oxynitrides and oxychalcogenides have been studied for photocatalytic degradation [5–8]. Recently, bismuth oxychalcogenides (BOXs) have emerged as novel semiconductors for their application in optoelectronics and photocatalysis [9-12]. Among which, bismuth oxysulfide (Bi2O2S) is a semiconductor with an indirect bandgap of ~1.1 eV and has excellent air stability [13]. Bi₂O₂S offers a long carrier lifetime, excellent charge dissociation and transport properties, which makes it a potential candidate for photocatalytic and photodetection applications. So far, only a limited number of reports have explored the photocatalytic activity of nanocomposites containing Bi₂O₂S [14-16]. However, the photocatalytic properties of standalone Bi₂O₂S nanosheets for dye degradation have not been previously reported. Herein, we report the photocatalytic behavior of Bi2O2S nanosheets for the oxidative photodegradation of organic pollutants under visible light. Congo red (CR) and rose bengal (RB) were chosen for this study due to their widespread industrial use, environmental challenges, and notable efficiency in our dye degradation experiment's initial screening.

2. Experimental

CR and RB were purchased from Fisher Scientific. $Bi(NO_3)_3 \cdot 5H_2O$, CH_4N_2S , KOH, NaOH, and cupric nitrate (CN) or $Cu(NO_3)_2 \cdot 3H_2O$ (99–104 %) were purchased from Sigma-Aldrich. Isopropyl alcohol (IPA), benzoquinone (BQ), and disodium ethylenediaminetetraacetate acid (Na₂-EDTA) were purchased from VWR. Bi_2O_2S nanosheets were synthesized using a simple solution process in ambient conditions. The detailed synthesis process is described in Fig. S1, (supporting information). Further, the structural, optical, morphological and photocatalytic characterizations were performed. Visible light irradiation experiments for photocatalytic degradation were conducted using an LS-150-Xe system with a cutoff filter L42 (Newport Corporation). The spectra were recorded using a VWR UV3100-PC UV–visible spectrophotometer.

3. Result and discussion

3.1. Material characterizations

Fig. 1a depicts the crystal structure of layered $\mathrm{Bi}_2\mathrm{O}_2\mathrm{S}$, which comprises alternative layers of bismuth oxide ($\mathrm{Bi}_2\mathrm{O}_2\mathrm{)}^{2+}$ and sulfur (S^2). The atomic model is designed using the 3D visualization tool VESTA and the source file was imported from the materials project library. Fig. 1b shows the XRD pattern of $\mathrm{Bi}_2\mathrm{O}_2\mathrm{S}$ nanosheet powder, where the indexed peaks confirm its orthorhombic phase (JCPDS # 00–034-1493). Fig. 1c shows the UV–Vis-DRS spectra of $\mathrm{Bi}_2\mathrm{O}_2\mathrm{S}$ nanosheets and the value of bandgap obtained using the Kubelka Munk function as shown in Fig. 1c (inset). The calculated value of the bandgap of $\mathrm{Bi}_2\mathrm{O}_2\mathrm{S}$ is ~ 1.17 eV.

E-mail address: fyan@nccu.edu (F. Yan).

a Department of Chemistry and Biochemistry, North Carolina Central University, Durham, NC 27707, United States of America

^b Materials Characterization Laboratory, Pennsylvania State University, University Park, PA 16802, United States of America

Fig. 1d show the FESEM image of Bi $_2O_2S$ nanosheets indicating the morphology of the material and confirming the nanosheet formation with the lateral dimensions of ≥ 100 nm. The elemental mapping image and atomic ratio of Bi $_2O_2S$ nanosheets was obtained using EDS (see Fig. S2, supplementary information). Fig. 1e shows the TEM image of Bi $_2O_2S$ nanosheets indicating the standalone nanosheets with weak electrostatic force between the layers.

3.2. Photocatalytic degradation studies

The UV–visible spectra of 30 ppm of CR and RB were recorded with and without $\rm Bi_2O_2S$ photocatalyst as shown in Fig. 2a-d. Fig. 2a and 2b show the degradation of CR and RB without photocatalysts respectively. From the UV–visible spectra, we observe the $\sim\!16$ % and $\sim\!49.5$ % degradation of CR and RB dyes, respectively. After controlled degradation, $\rm Bi_2O_2S$ nanosheet powder (1 mg/mL) was added to both the dye solution and stirred for 45 min in the dark to obtain equilibrium. The photodegradation was carried out under a 150 W Xe arc lamp with a UV filter to pass only visible light. The same time intervals were kept for degradation studies as for control degradation shown in Fig. 2c-d. The photodegradation for CR and RB was $\sim\!82$ % and $\sim\!80.6$ % as shown in Fig. 2c and 2d respectively. The degradation values adhere to a first-order pseudo-kinetic model, as represented by the following equation:

$$\ln(C_t/C_o) = -kt \tag{1}$$

where Co is the equilibrium concentration of the reaction solution before

irradiation, and C_t is the concentration of the reaction solution at reaction time (t). The photodegradation processes of CR and RB in all their respective photocatalysts, as depicted in Fig. 3a and 3b respectively. The degradation rate constant (k) values for the degradation of CR and RB dyes were determined to be 1.8×10^{-2} min⁻¹ and 1.3×10^{-2} min⁻¹.

3.3. Scavenger test and degradation mechanism

Fig. 4a shows the effect of IPA, BQ, Na₂-EDTA, and CN on the photocatalytic degradation of CR dye by Bi₂O₂S nanosheets. These scavengers help to find the dominant radicals responsible for degradation [17]. Bi₂O₂S nanosheets exhibited \sim 82 % degradation efficiency without any scavengers. The inclusion of IPA, EDTA, BQ, and CN led to a decrease in the degradation efficiency, yielding percentages of 24.3 %, 41 %, 54.6 %, and 36 % respectively. The findings confirm the dominance of \bullet OH radicals in photodegrading CR. The valence band (VB) potential of Bi₂O₂S was reported at 1.81 V vs. the reversible hydrogen electrode (RHE).[18] The conduction band (CB) potential was calculated by combining the bandgap (1.17 eV) and the calculated CB potential was 0.64 V vs. RHE.

The photodegradation mechanism as shown in Fig. 4b can be expressed as follows: when visible light irradiates Bi_2O_2S nanosheets, electron-hole pairs are generated on the surface. The adsorbed water and hydroxyl molecules react with generated charge carriers to form ${}^{\bullet}$ OH radicals. The effective interaction between these radicals and dye molecules leads to the degradation of the dye.

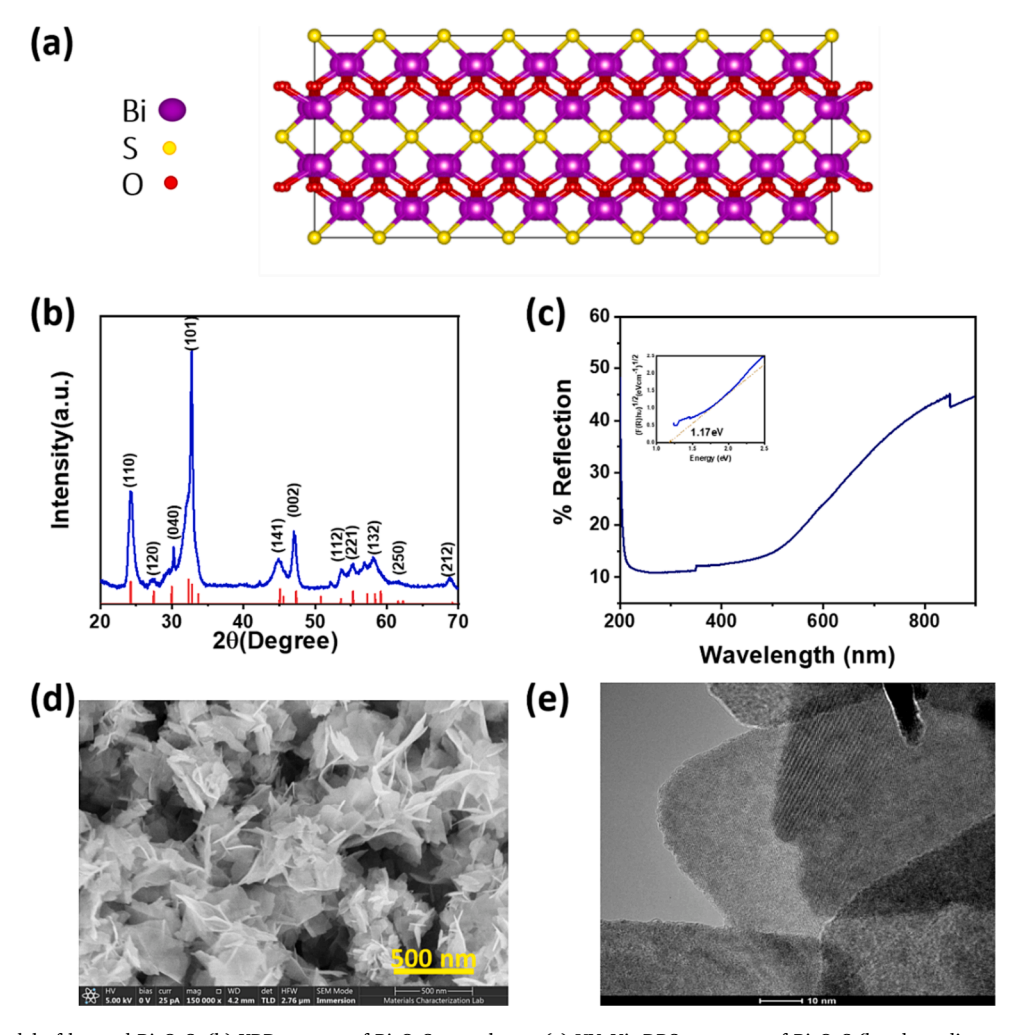


Fig. 1. (a) Atomic model of layered Bi_2O_2S , (b) XRD pattern of Bi_2O_2S nanosheets, (c) UV-Vis-DRS spectrum of Bi_2O_2S (bandgap diagram), (d) FESEM image of Bi_2O_2S nanosheets, and (e) TEM image of Bi_2O_2S nanosheets.

T.R. Seling et al. Materials Letters 361 (2024) 136136

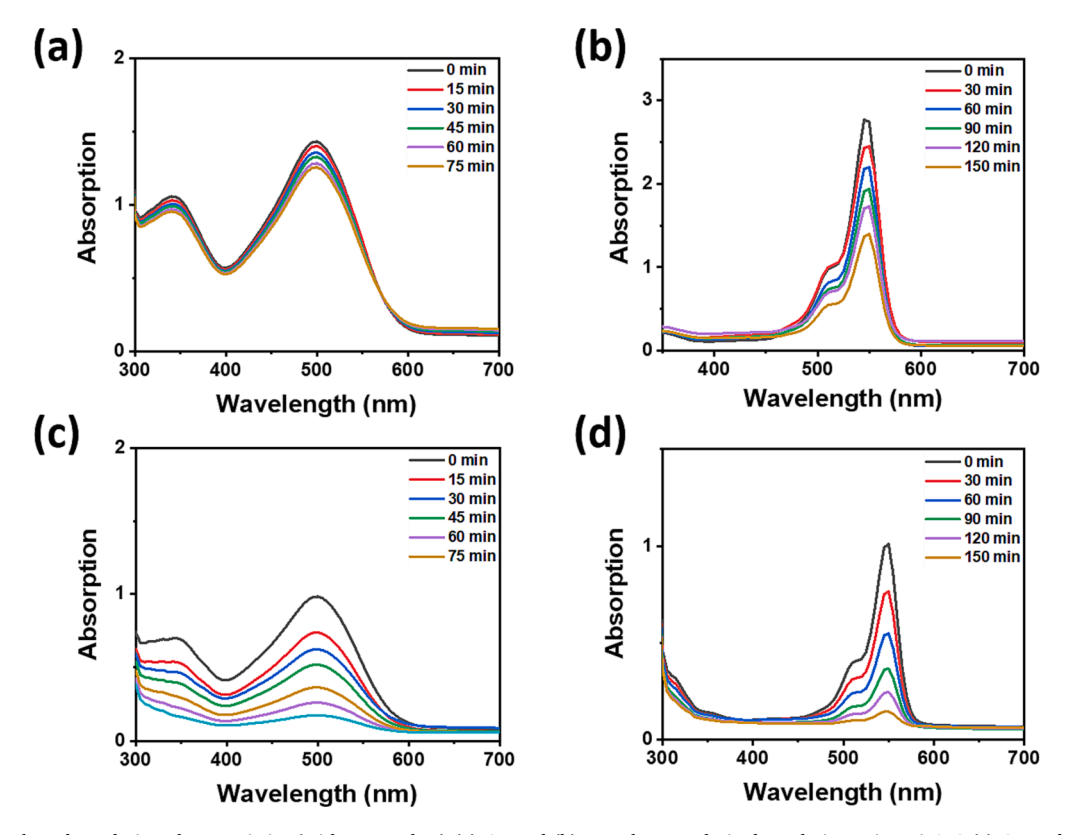


Fig. 2. Photodegradation characteristics (without catalyst) (a) CR and (b) RB. Photocatalytic degradation using Bi_2O_2S (c) CR and (d) RB.

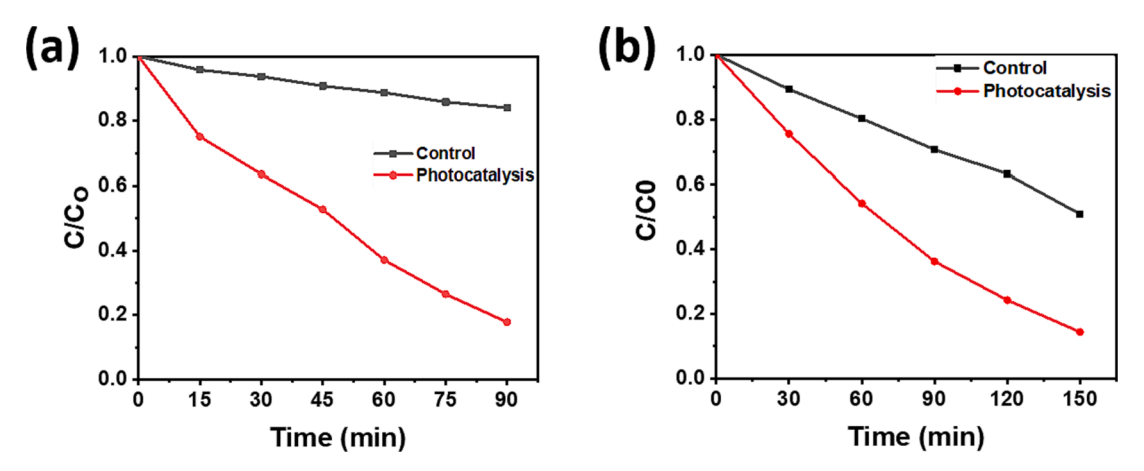


Fig. 3. C/C_o plots for (a) CR and (b) RB.

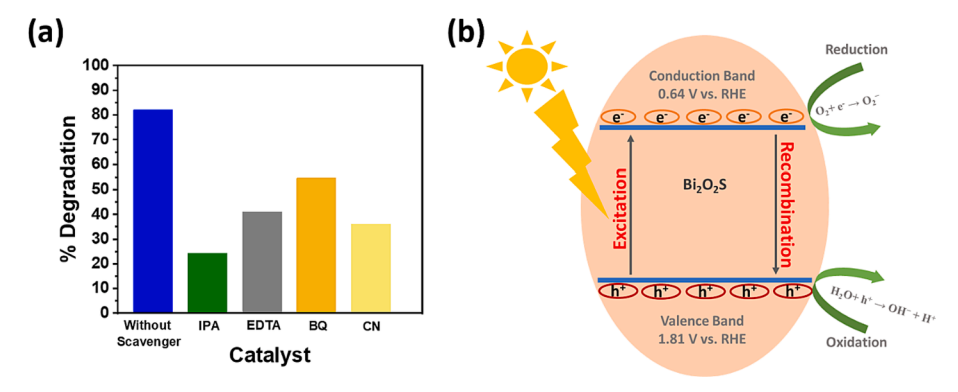


Fig. 4. (a) Percent degradation of CR dye in the presence of different scavengers, and (b) schematic representation of photocatalytic degradation mechanism.

$$Bi_2O_2S + h\nu \rightarrow e^- + h^+ \tag{2}$$

$$H_2O + h^+ \to OH^- + H^+$$
 (3)

$$OH^- + h^+ \rightarrow \cdot OH \tag{4}$$

$$Dye + \cdot OH \rightarrow Dye \ degradation \ products$$
 (5)

It is noteworthy that the decrease in dye absorption observed in the presence of Bi_2O_2S nanosheets is partially influenced by photoreduction. The reduction in dye absorption under visible light is a complex phenomenon influenced by various factors, such as electronic transitions, photochemical reactions, conformational changes, photodegradation, and solvent effects.

4. Conclusions

To summarize, we have investigated the photocatalytic properties of ultrathin $\rm Bi_2O_2S$ nanosheets. The structural, optical and morphological characterizations confirm the crystalline phase, band gap and nanostructure of the synthesized nanosheets. $\rm Bi_2O_2S$ nanosheets show ${\sim}82\,\%$ and ${\sim}80.6\,\%$ degradation efficiency for CR and RB dyes under visible light illumination. The report shows the potential of the $\rm Bi_2O_2S$ nanosheets as efficient catalysts that can be used for the treatment of effluents and water sources.

CRediT authorship contribution statement

Tank R. Seling: Data curation, Investigation, Methodology. Amit Kumar Shringi: Data curation, Writing – original draft, Investigation, Formal analysis. Ke Wang: Data curation, Methodology. Ufana Riaz: Methodology, Project administration, Resources. Fei Yan: Conceptualization, Funding acquisition, Project administration, Resources, Supervision, Writing – review & editing.

Declaration of competing interest

The authors declare that they have no known competing financial interests or personal relationships that could have appeared to influence the work reported in this paper.

Data availability

Data will be made available on request.

Acknowledgements

The authors thank the financial support by the U.S. National Science Foundation (Award #2122044). This research was partially sponsored by the Army Research Office (ARO) and was accomplished under Grant W911NF2210109. The views and conclusions contained in this document are those of the authors and should not be interpreted as representing the official policies, either expressed or implied, of the ARO or the U.S. Government. The U.S. Government is authorized to reproduce and distribute reprints for Government purposes notwithstanding any copyright notation herein.

Appendix A. Supplementary data

Supplementary data to this article can be found online at https://doi.

org/10.1016/j.matlet.2024.136136.

References

- M.K. Purkait, V.D. Kumar, D. Maity, Treatment of leather plant effluent using NF followed by RO and permeate flux prediction using artificial neural network, Chem. Eng. J. 151 (2009) 275–285, https://doi.org/10.1016/j.cej.2009.03.023.
- [2] T.S. Natarajan, M. Thomas, K. Natarajan, H.C. Bajaj, R.J. Tayade, Study on UV-LED/TiO₂ process for degradation of Rhodamine B dye, Chem. Eng. J. 169 (2011) 126–134, https://doi.org/10.1016/j.cej.2011.02.066.
- [3] P. Chanikya, P.V. Nidheesh, D. Syam Babu, A. Gopinath, M. Suresh Kumar, Treatment of dyeing wastewater by combined sulfate radical based electrochemical advanced oxidation and electrocoagulation processes, Sep. Purif. Technol. 254 (2021) 117570, https://doi.org/10.1016/j.seppur.2020.117570.
- [4] S. Alhammadi, B.G. Mun, S. Gedi, V.R. Minnam Reddy, A.M. Rabie, M.S. Sayed, J.-J. Shim, H. Park, W.K. Kim, Effect of silver doping on the properties and photocatalytic performance of In₂S₃ nanoparticles, J. Mol. Liq. 344 (2021) 117649, https://doi.org/10.1016/j.molliq.2021.117649.
- [5] S. Gautam, H. Agrawal, M. Thakur, A. Akbari, H. Sharda, R. Kaur, M. Amini, Metal oxides and metal organic frameworks for the photocatalytic degradation: A review, J. Environ. Chem. Eng. 8 (2020) 103726, https://doi.org/10.1016/j.ieee.2020.103726
- [6] S. Huang, C. Chen, H. Tsai, J. Shaya, C. Lu, Photocatalytic degradation of thiobencarb by a visible light-driven MoS₂ photocatalyst, Sep. Purif. Technol. 197 (2018) 147–155. https://doi.org/10.1016/j.seppur.2018.01.009.
- [7] E. Martínez-Ferrero, Y. Sakatani, C. Boissière, D. Grosso, A. Fuertes, J. Fraxedas, C. Sanchez, Nanostructured titanium oxynitride porous thin films as efficient visible-active photocatalysts, Adv. Funct Mater. 17 (2007) 3348–3354, https://doi. org/10.1002/adfm.200700396.
- [8] D. Vrushabendrakumar, H. Rajashekhar, S. Riddell, A.P. Kalra, K.M. Alam, K. Shankar, Synthesis, characterization, and visible light photocatalytic activity of solution-processed free-standing 2D Bi₂O₂Se nanosheets, Nanotechnology. 32 (2021) 485602, https://doi.org/10.1088/1361-6528/ac1753.
- [9] B. Chitara, E. Dimitrov, M. Liu, T.R. Seling, B.S.C. Kolli, D. Zhou, Z. Yu, A. K. Shringi, M. Terrones, F. Yan, Charge transfer modulation in vanadium-doped WS₂/Bi₂O₂Se heterostructures, Small. (2023) 2302289, https://doi.org/10.1002/smll.202302289.
- [10] Y. Luo, H. Han, G. Zhang, Q. Wang, Y. Jia, Construction of Z-scheme a-Fe₂O₃/graphene/Bi₂O₂S heterojunction for visible-light-driven photocatalytic CO₂ conversion, Sep. Purif. Technol. 314 (2023) 123607, https://doi.org/10.1016/j.sepnur.2023.123607.
- [11] X. Yang, L. Qu, F. Gao, Y. Hu, H. Yu, Y. Wang, M. Cui, Y. Zhang, Z. Fu, Y. Huang, W. Feng, B. Li, P. Hu, High-performance broadband photoelectrochemical photoelectors based on ultrathin Bi₂O₂S nanosheets, ACS Appl. Mater. Interfaces. 14 (2022) 7175–7183. https://doi.org/10.1021/acsami.1e22448.
- [12] B. Chitara, A.K. Shringi, B. Roy, M.H. Wu, F. Yan, Facile synthesis and morphology-induced photoconductivity modulation of Bi₂O₂S nanostructures, Mater. Lett. 346 (2023) 134545, https://doi.org/10.1016/j.matlet.2023.134545.
- [13] X. Zhang, Y. Liu, G. Zhang, Y. Wang, H. Zhang, F. Huang, Thermal decomposition of bismuth oxysulfide from photoelectric Bi₂O₂S to superconducting Bi₄O₄S₃, ACS Appl. Mater. Interfaces. 7 (2015) 4442–4448, https://doi.org/10.1021/ am502150
- [14] A.L. Pacquette, H. Hagiwara, T. Ishihara, A.A. Gewirth, Fabrication of an oxysulfide of bismuth Bi₂O₂S and its photocatalytic activity in a Bi₂O₂S/In₂O₃ composite, J. Photochem. Photobiol. a: Chemistry. 277 (2014) 27–36, https://doi.org/10.1016/j.jphotochem.2013.12.007.
- [15] Y. Luo, H. Han, J. Li, Q. Wang, W. Zhang, Y. Jia, Fe doped Bi₂O₂S nanosheets for improved organic pollutants photo-Fenton degradation and CO₂ photoreduction, Sep. Purif. Technol. 306 (2023) 122734, https://doi.org/10.1016/j. sepnur.2022.122734.
- [16] L. Jiang, Z. Li, D. Wang, T. Guo, Y. Hu, In-situ growth of p-type Ag₂O on n-type Bi₂O₂S with intimate interfacial contact for NIR light-driven photocatalytic CO₂ reduction, Appl. Surf. Sci. 601 (2022) 154185, https://doi.org/10.1016/j.apsusc.2022 154185
- [17] K. Sahu, J. Singh, S. Mohapatr, Photocatalytic and catalytic removal of toxic pollutants from water using CuO nanosheets, J. Mater. Sci. Mater. Electron. 30 (2019) 6088–6099, https://doi.org/10.1007/s10854-019-00910-3.
- [18] W. Zhang, D. Liu, W. Jin, D. Zhang, T. Sun, E. Liu, X. Hu, H. Miao, In-situ construction of 2D/ID Bi₂O₂S/Bi₂S₃ heterojunction from the topological transformation of Bi₂O₂S with significantly enhanced photoelectrochemical performance, Int. J. Hydrogen Energ. 51 (2024) 1545–1557, https://doi.org/10.1016/j.ijhydene.2023.09.253.